Journal of Magnetic Resonance **139,** 334–341 (1999)
Article ID jmre.1999.1777, available online at http://www.idealibrary.com on IDEAL®

# Measurement of Convection and Temperature Profiles in Liquid Samples

Nikolaus M. Loening and James Keeler[1]

*Department of Chemistry, University of Cambridge, Lensfield Road, Cambridge CB2 1EW, United Kingdom*

Received December 18, 1998; revised March 17, 1999

**This paper describes a method for measuring the rate of convective flow in a liquid sample used for high-resolution NMR. The measurement is straightforward and achieves a clean separation of convection from other effects such as diffusion and relaxation. Convection results from temperature gradients within the sample, and it is shown how these can be measured with the aid of a simple chemical shift imaging experiment of a sample whose spectrum shows a strong and well characterized temperature dependence. The use of these two methods is illustrated by showing how the rate of convection and the temperature profile depend on the solvent, temperature, and gas flow rate of the temperature regulating system. It is also shown that broadband $^{13}C$ decoupling results in significant temperature gradients and associated convection.** 

*Key Words:* **convection; stimulated echo; temperature imaging; gradients.**

## INTRODUCTION

It has been recognized for some time that the quality of high-resolution NMR spectra is degraded by temperature gradients which result from poor temperature stabilization of the sample. The elegant work of Allerhand *et al.* on "ultra high resolution NMR" is a particularly striking demonstration of the important role that temperature control plays (*1*, *2*). Not surprisingly, therefore, obtaining good temperature control is a crucial factor in the design of NMR probes and variable temperature units.

In this paper we introduce two experimental methods which make it possible to measure, quantitatively and in a straightforward manner, the temperature profile in the sample and the rate of convective flow which is often a consequence of an uneven temperature profile. As has recently been shown by Jerschow and Müller (*3*, *4*) the presence of convection in the sample is particularly deleterious to experiments which use pulsed field gradients for coherence pathway selection. So, even if the resolution of the spectrum is not significantly affected by the temperature gradients, the associated convection can result in a loss of signal. We present measurements on some typical NMR samples showing the effect of solvent viscosity, temperature, and flow-rate of the temperature regulating gas on both the temperature profile and the rate of convection.

[1] To whom correspondence should be addressed. E-mail: James.Keeler@ch.cam.ac.uk, Fax: +44 1223 336913.

## THEORY

### *Compensation of Convection Effects on Coherence Selection Using Gradients*

This work is concerned with convection parallel to the long axis (the *z*-axis) of an NMR sample. In such a case, convection can be envisaged as an upward movement of less dense (hotter) liquid, thereby displacing cooler liquid. A temperature gradient is necessary to create the differences in density which result in convection. Convective flow has a laminar component, which involves the steady movement of liquid, and a turbulent component; we will only be concerned with laminar flow.

Convective flow only takes place when the temperature gradient exceeds a critical value which depends on, among other things, the shape of the sample, the viscosity and thermal expansivity of the liquid, and the acceleration due to gravity (the motion in the vertical direction is against gravity). A simple calculation based on the modified Rayleigh–Bénard equation indicates that, for a solvent such as chloroform, a temperature gradient of as little as 0.05 K $cm^{-1}$ is sufficient to cause convective flow. In general, larger temperature gradients are needed for more viscous solvents.

As convection results in the physical movement of the spins it interferes with the formation of gradient spin echoes, in the same way in which diffusion interferes; coherence selection using gradients is also affected. However, the ordered nature of convection makes it possible to use modified pulse and gradient sequences to compensate for its effects; this is in marked contrast to diffusion, a random process, whose effects cannot be compensated.

In the context of NMR imaging, Callaghan *et al.* have shown how it is possible to devise pulse sequences which, to some degree, undo the effects of convection on gradient refocusing experiments (*5*). More recently, Jerschow and Müller have shown that the idea of *convection compensation*—that is, pulse



1090-7807/99 $30.00

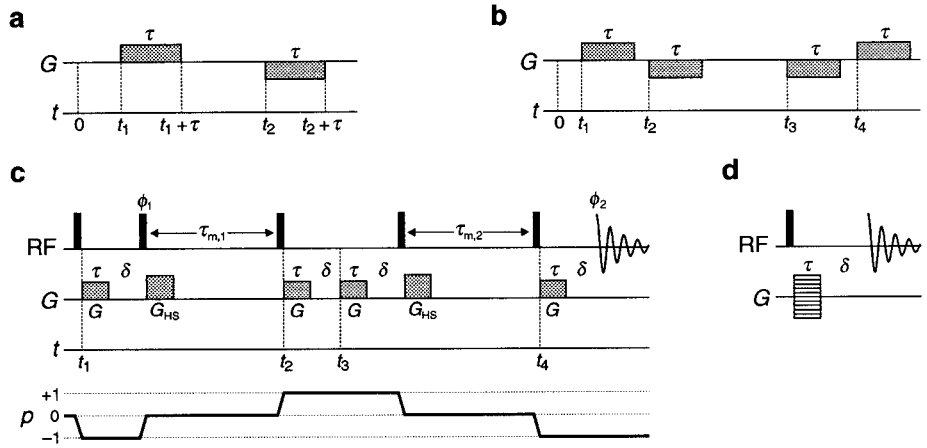


**FIG. 1.** Gradient and pulse sequences used in this work. Pulses are shown on the line marked RF and gradients on the line marked *G*; time markers for some of the sequences are shown on the line marked *t*. For sequence (c), the selected coherence transfer pathway is shown beneath it. All pulses have 90° flip angles and phase *x* unless otherwise noted. Sequence (a) is a simple gradient refocusing scheme, which is not convection compensated, and sequence (b) is a more complex scheme which is convection compensated provided $(t_2 - t_1) = (t_4 - t_3)$; see text for further details. Sequence (c) is the one advocated in this paper for the measurement of convection velocity profiles. The phases $\phi_1$ and $\phi_2$ are cycled $x, y, -x, -y$ and $x, -y, -x, y$, respectively. Sequence (d) is a chemical shift imaging experiment which can be used in conjunction with a compound whose spectrum is temperature sensitive to measure temperature profiles.

sequence elements designed to cancel the effects of convection on refocusing—can be included to advantage in a number of high-resolution NMR experiments (*3, 4*). Our method for measuring flow is based on the idea of convection compensation so this will be described in some detail.

When pulsed field gradients are used for coherence selection, first a defocusing gradient is applied; the result is that the coherence acquires a *spatially dependent* phase. Then a coherence transfer step follows, and finally a second refocusing gradient designed to undo exactly the spatially dependent phase caused by the first gradient. The size of the spatially dependent phase is determined by the coherence order, the shape, strength, and length of the gradient and, as its name implies, the position of the spin (or spins) in the sample. For the second gradient to undo exactly the phase induced by the first, and therefore refocus the required coherence pathway, the spins must remain immobile during the gradients and the period between them. With any movement to a new position the spins will experience a spatially dependent phase during the second gradient different from that needed to undo the effect of the first gradient. The result will be a loss of signal.

The basic idea needed to analyze the effect of a gradient in the presence of convective flow is that of the *velocity dependent phase*. This is a phase, additional to the spatially dependent part, which is acquired because the spins *move* during a gradient and so experience a varying magnetic field. If the gradient is assumed to give rise to a linear variation in magnetic field along $z$, with magnitude $G(t)$ at time $t$ (for example, $G$ might be in T m$^{-1}$ or G cm$^{-1}$), the strength of the magnetic field at position $z(t)$ due to the gradient is $G(t)z(t)$. The phase acquired by a coherence of order $p$ at position $z(t)$ between time $t$ and $t + dt$ is given by

$$\gamma p G(t)\, z(t) dt,$$

where $\gamma$ is the gyromagnetic ratio. If it is assumed that the spins are moving in the $z$-direction with velocity $v$, $z(t)$ can be written as $z_0 + vt$, where $z_0$ is the initial position at the start of the pulse sequence (time 0). A gradient pulse of length $\tau$ is applied, and for generality it will be assumed that this starts at time $t_1$. The total phase acquired at the end of the gradient pulse is given by

$$\begin{aligned}\int_{t_1}^{t_1+\tau} \gamma p G(t)[z_0 + vt]dt &= \int_{t_1}^{t_1+\tau} \gamma p G(t) z_0 dt + \int_{t_1}^{t_1+\tau} \gamma p G(t) vt dt \\ &= \phi_0 + \phi_v.\end{aligned}$$

On the second line the first integral is the usual spatially dependent phase, $\phi_0$; the second integral is the velocity dependent phase, $\phi_v$. In the case of a square-profiled gradient of strength $G_0$ these phases are $\phi_0 = \gamma p G_0 z_0 \tau$ and $\phi_v = \frac{1}{2}\gamma p G_0 v(2t_1\tau + \tau^2)$. In the latter phase, the term in $\tau^2$ is due to the movement during the gradient, and the term in $t_1\tau$ is attributable to the movement which has already taken place prior to application of the gradient.

The simplest refocusing scheme is to imagine applying the first gradient, of length $\tau$ and strength $G_0^{(1)}$, at time $t_1$, then applying a second gradient of equal length and of strength $G_0^{(2)}$ at time $t_2$; this sequence is shown in Fig. 1a. The spatially dependent, $\phi_0^{(i)}$, and velocity dependent, $\phi_v^{(i)}$, phases due to the first and second gradients are

$$\phi_0^{(1)} = \gamma p G_0^{(1)} z_0 \tau, \quad \phi_v^{(1)} = \tfrac{1}{2}\gamma p G_0^{(1)} v(2t_1\tau + \tau^2)$$
$$\phi_0^{(2)} = \gamma p G_0^{(2)} z_0 \tau, \quad \phi_v^{(2)} = \tfrac{1}{2}\gamma p G_0^{(2)} v(2t_2\tau + \tau^2),$$

where for simplicity it has been assumed that the gradients have a square profile and that the coherence order has not changed. In the absence of convection ($v = 0$), setting $G_0^{(2)} = -G_0^{(1)}$ will ensure complete refocusing as the two velocity independent phases, $\phi_0^{(1)}$ and $\phi_0^{(2)}$, cancel and the velocity dependent phases go to zero. If there is convection, the velocity dependent phases do not go to zero but leave a phase

$$\begin{aligned}\phi_v^{(1)} + \phi_v^{(2)} &= \tfrac{1}{2}\gamma p G_0^{(1)} v(2t_1\tau + \tau^2) \\ &\quad - \tfrac{1}{2}\gamma p G_0^{(1)} v(2t_2\tau + \tau^2) \\ &= \gamma p G_0^{(1)} v\tau(t_1 - t_2). \qquad [1]\end{aligned}$$

This unwanted phase depends on the velocity, the duration of the gradients and, most importantly, the *separation in time* of the two gradients.

The key to removing this unwanted phase error is to apply two further gradients: the third starts at time $t_3$ and is in the same sense as the second gradient, and the fourth is applied at time $t_4$ and is in the same sense as the first: i.e., $G_0^{(3)} = -G_0^{(1)}$ and $G_0^{(4)} = G_0^{(1)}$; this sequence is shown in Fig 1b. Clearly, in the absence of convection, the third and fourth gradients will refocus one another. In the presence of convection, the velocity dependent phase arising from the third and fourth gradients is

$$\begin{aligned}\phi_v^{(3)} + \phi_v^{(4)} &= -\tfrac{1}{2}\gamma p G_0^{(1)} v(2t_3\tau + \tau^2) \\ &\quad + \tfrac{1}{2}\gamma p G_0^{(1)} v(2t_4\tau + \tau^2) \\ &= -\gamma p G_0^{(1)} v\tau(t_3 - t_4).\end{aligned}$$

This can be made equal and opposite to the velocity dependent phase resulting from the first two gradients by ensuring that

$$(t_2 - t_1) = (t_4 - t_3).$$

In words, the condition for compensation is that the velocity dependent phase resulting from the first pair of gradients, Eq. [1], be canceled by that from the second pair. In this example, this condition is met by making the separation between the two pairs of gradients the same, but there are other possibilities which involve varying the strength of the gradients.

This method of compensation is visualized graphically in Fig. 2. The diagram shows the magnetic field, due to the gradient as a function of time, which is experienced by a small volume element of spins assumed to be moving with a steady velocity. Distance, and hence the magnetic field due to the gradient, is thus directly proportional to time. Two lines are shown: one for a positive gradient ($+G$) and one for a negative one ($-G$).

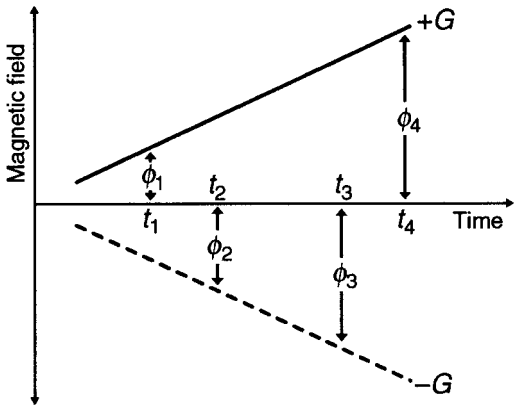


**FIG. 2.** Visualization of the mechanism of convection compensation by the gradient sequence of Fig. 1b. The plot shows the magnetic field due to the gradient pulse experienced by a volume element of spins which is moving with a steady velocity in the direction of the gradient. The solid line, marked $G$, is for a positive gradient and the dashed line, marked $-G$, is for a negative gradient. The phases acquired by the spins at times $t_1$, $t_2$, $t_3$, and $t_4$ are proportional to the strength of the magnetic field at these times; note that the second and third gradients are applied in the sense opposite to that of the first and fourth, so the magnetic field for the former two is given by the dashed line. Provided that $(t_2 - t_1) = (t_4 - t_3)$ the phases will cancel and the signal will be refocused without loss; see text for further discussion.

The phase experienced by a coherence is proportional to the magnetic field, which is proportional to distance and hence, in this case, time. For simplicity, motion during the gradient is ignored, so that the phase, $\phi_1$, acquired during the first gradient placed at time $t_1$ is simply proportional to the magnetic field at that time. The phase acquired during the other three gradients is likewise proportional to the magnetic fields at the times they are applied, with the proviso that the gradient direction be reversed for the second and third gradients. Inspection of the diagram shows clearly that the difference $(\phi_2 - \phi_1)$ will be equal and opposite to the difference $(\phi_4 - \phi_3)$ provided that $(t_2 - t_1)$ is equal to $(t_4 - t_3)$; the separation of time points $t_2$ and $t_3$ is irrelevant. This is the condition for convection compensation outlined above.

Generalizing this argument for arbitrary gradient sequences, the condition for compensation is that the velocity dependent phases cancel, which requires that

$$\sum_i \int_{t_i}^{t_i+\tau_i} \gamma p_i G^{(i)}(t) v t dt = 0,$$

where the index $i$ indicates the $i$th gradient, starting at time $t_i$ and of duration $\tau_i$. The factors of $\gamma$ (for the homonuclear case) and $v$ cancel so the compensation condition can be expressed more compactly as

$$\sum_i \int_{t_i}^{t_i+\tau_i} p_i G^{(i)}(t) t dt = 0.$$

In words, this says that the first moment of the effective gradients must be zero, where the effective gradient is the gradient strength multiplied by the coherence order. This condition assumes that a given spin moves at a constant velocity throughout the experiment; if there is any change, the compensation is incomplete.

*Measurement of Convection Velocity Profiles*

If refocusing is imperfect due to convection, the result will be that the signal acquires a phase shift dependent on the velocity, the strength of the gradient, and the timing in the sequence. In practice, there will usually be a distribution of velocities and, when summed across the whole sample, the resulting distribution of phases usually results in an attenuation of the amplitude of the signal. In principle it ought to be possible to measure the velocity distribution from this signal attenuation—for example, by measuring it as a function of the length or strength of the gradients. However, there are other factors, such as diffusion and relaxation, which also cause attenuation of the signal in such an experiment; it would be desirable to be able to separate these effects.

Figure 1c shows a pulse sequence which we have devised which makes it possible to measure *just the part of the signal attenuation due to convection.* It will be shown that if one of the mixing times is decreased while the other is increased in concert the resulting signal attenuation is solely due to convection.

Basically the sequence consists of two stimulated echoes, with mixing times $\tau_{m,1}$ and $\tau_{m,2}$. The gradients $G$ select the coherence transfer pathway shown, and the gradients $G_{HS}$ are used to destroy all but $z$-magnetization present during the mixing times. The second gradient $G$ refocuses the first, and likewise the fourth refocuses the third. The gradients are of duration $\tau$ and the times $\delta$ are small delays to enable the homogeneity to recover after the gradient pulses.

In contrast to the simple sequence of Fig. 1b, all the gradients in the sequence of Fig. 1c are in the same sense, so that the pathway which is refocused is one in which the coherence order present during the refocusing gradient is opposite in sign to the coherence present during the defocusing gradient; this is indicated by the accompanying coherence transfer pathway. The two sequences are entirely equivalent with respect to the effects of convection. The change in coherence order is needed in the sequence of Fig. 1c in order for chemical shift evolution during the times when the magnetization is transverse to be refocused at the end of the sequence.

The four gradient pulses start at times $t_1 \cdots t_4$, where

$$t_1 = 0, \quad t_2 = \tau + \delta + \tau_{m,1},$$

$$t_3 = 2\tau + 2\delta + \tau_{m,1}, \quad t_4 = 3\tau + 3\delta + \tau_{m,1} + \tau_{m,2},$$

from which it follows that

$$(t_2 - t_1) = \tau + \delta + \tau_{m,1} \quad \text{and} \quad (t_4 - t_3) = \tau + \delta + \tau_{m,2}.$$

From the above discussion it is clear that these quantities are equal, and the sequence convection compensated, when $\tau_{m,1} = \tau_{m,2}$. Note that, in contrast to the sequence of Fig. 1b, all the gradients are applied in the same sense; however, the coherence order is $-1$ during the first and fourth gradients, and $+1$ during the second and third. Effectively, the spins experience the second and third gradients in the opposite sense, as required to refocus the spatially dependent phase.

The total velocity dependent phase for the sequence is

$$\phi_v^{tot} = \gamma G_0 v \tau(\tau_{m,1} - \tau_{m,2}),$$

where it has been assumed that all the gradients have a square profile and are of the same strength, $G_0$. Note that this phase does not depend on the position of the spins in the sample, and that because the gradients have been assumed to be of the same length there is no term in $\tau^2$ as the velocity dependent phases which accrue during the gradients cancel (see Eq. [1]). For non-square gradients with shape factor $s$, the phase simply becomes $\phi_v^{tot} = \gamma s G_0 v \tau(\tau_{m,1} - \tau_{m,2})$. The shape factor is the area under the gradient profile, normalized so that a square-shaped gradient has $s = 1$; for gradients shaped to a half sine-bell, $s = 2/\pi$.

The key point is that this velocity dependent phase depends on the difference in the two mixing times, whereas effects such as diffusion and relaxation will depend on the sum of the mixing times. By altering the timing in such a way that the sum of these two times remains constant, but the difference between them varies, we achieve an experiment in which the signal attenuation depends solely on convection. If the difference in the two mixing times is $\Delta$, and their sum is $T$, the two mixing times are

$$\tau_{m,1} = \tfrac{1}{2}(T + \Delta) \quad \text{and} \quad \tau_{m,2} = \tfrac{1}{2}(T - \Delta).$$

To find an expression for the signal, $S$, from the sample, account needs to be taken of the possibility that the convection velocity may not be constant, but distributed in some way. If $f(v)$ describes the probability distribution of the convection velocity, then the signal is

$$S(\Delta) = k \int_{-\infty}^{\infty} f(v) \exp(i\phi_v^{tot}) dv$$

$$= k \int_{-\infty}^{\infty} f(v) \exp(i\gamma s G_0 v \tau \Delta) dv, \qquad [2]$$

where $k$ is a constant. The simplest assumption is that the velocity distribution is constant in the range $-v_{max}$ to $v_{max}$. In this case, the signal is

$$\frac{S(\Delta)}{S_0} = \frac{\sin(\gamma s G_0 v_{max} \tau \Delta)}{\gamma s G_0 v_{max} \tau \Delta},$$

where $S_0$ is the signal when $\Delta = 0$. As a function of the time $\Delta$ the normalized signal varies as a sinc function; assuming that the gradient strength is known, there is just one parameter to fit the experimental data, that is, the maximum velocity. The analysis shows how the experiment achieves a clean separation of convection from other effects.

For the general case, it is seen from Eq. [2] that by recognizing $\gamma s G_0 v \tau$ as a frequency, $\omega$, $S(\Delta)$ is the inverse Fourier transform of $f(\omega)$

$$S(\Delta) = \frac{k}{\gamma s G_0 \tau} \int_{-\infty}^{\infty} f(\omega) \exp(i\omega\Delta) d\omega$$

$$= \frac{k}{\gamma s G_0 \tau} FT^{-1}[f(\omega)],$$

where $f(\omega)$ is the velocity probability distribution expressed in terms of $\omega$. It follows that $f(\omega)$ is the Fourier transform of $S(\Delta)$, multiplied by a scaling factor; the frequency axis is interpreted as $\gamma s G_0 v \tau$, which can be turned into a velocity provided that the gradient strength is known. From measurements of the signal decay it is thus possible to determine the velocity profile.

If $f(v)$ is symmetric about $v = 0$ then $S(\Delta)$ is real, i.e., it has pure phase. In our experiments we have not detected any phase shifts in $S(\Delta)$ which would indicate an unsymmetrical distribution of velocities.

### *Measurement of Temperature Profiles*

The approach to measuring temperature profiles that we have adopted is to record a two-dimensional chemical shift image of the sample tube. Essentially, such an image allows the measurement of a high-resolution spectrum at different positions in the sample. By choosing a compound with a well characterized temperature dependent spectrum the temperature can be measured. In our case, we were restricted to $z$-axis gradients, so the measurements are of average temperatures in a series of thin slices along the long axis of the sample tube.

The imaging sequence used is shown in Fig. 1d (*6*); the strength of the gradient is incremented in regular steps to generate the second dimension (analogous to $t_1$) and as no gradient is applied during acquisition a high-resolution spectrum is recorded. After double Fourier transformation cross sections parallel to $F_2$ through the resulting spectrum correspond to spectra taken from successive slices through the sample.

We have found that the thulium complex, thulium(III)-1,4,7,10-tetraazacyclododecane-1,4,7,10-tetrakis-(methylene phosphonate) complex (HTmDOTP), recently advocated by Zuo *et al.* (*7*), has a suitable temperature dependent spectrum. The compound is paramagnetic and shows proton resonances over the range −400 to 520 ppm; the several peaks have a strong and well documented temperature dependence, and the compound is water soluble. We chose to measure the temperature based on the separation between the two resonances at −155 and 73 ppm (at 300 K). By measuring a separation, rather than an absolute frequency, problems with $B_0$ shifts due to the gradients and imperfect shimming are removed; in addition, as these two peaks move in opposite directions when the temperature is changed the sensitivity of the measurement is improved.

One difficulty with HTmDOTP is that the lines are quite broad, typically 200–300 Hz, which reduced somewhat the accuracy to which their positions can be measured. Nevertheless, it is estimated that with SNR of around 100:1, typical in our experiments, it is possible to determine the frequency separations to within 1 Hz and hence determine temperature changes of as little as 0.01 K.

## RESULTS

All spectra were recorded using a Bruker DRX300 spectrometer equipped with a 5 mm dual probe; the radiofrequency coil is about 1 cm in length. The samples used were contained in standard 5 mm diameter tubes and were filled to a depth of *ca.* 6 cm. The temperature was regulated by means of a variable temperature unit consisting of a chiller which runs at a fixed temperature followed by a heating stage. The temperature was measured by means of a thermocouple located below the sample region. Measurements were also made on a Bruker DRX500 spectrometer, with very similar results.

### *Convection Measurements*

For the pulse sequence of Fig. 1c, typical experimental conditions are gradients, $G$, of strength 11.6 G cm$^{-1}$, duration 2 ms, and shaped to a half sine-bell. Total mixing times of 32 ms for nonviscous solvents such as $CHCl_3$ and 320 ms for more viscous solvents such as water and DMSO are typical; these enable $\Delta$ to be varied between −32 and +32 ms, and −320 and +320 ms, respectively.

Figure 3a shows results obtained using DMSO in DMSO-$d_6$ at a temperature of 320 K; a value of $\Delta$ somewhat larger than usual has been used so that the decay can be visualized clearly. The signal decay has the appearance of a sinc function, and fits moderately well to such a function, leading to an estimate of $v_{max}$ as 477 ± 5 $\mu$m s$^{-1}$. As discussed above, the model which leads to a sinc function for the signal attenuation assumes that the velocities are distributed evenly between $-v_{max}$ and $+v_{max}$. Fourier transformation of the decay gives a direct measure of this velocity distribution, and this is compared in Fig. 3b with the flat distribution based on fitting the decay to a sinc function. It can be seen that there is fair agreement in terms of the range

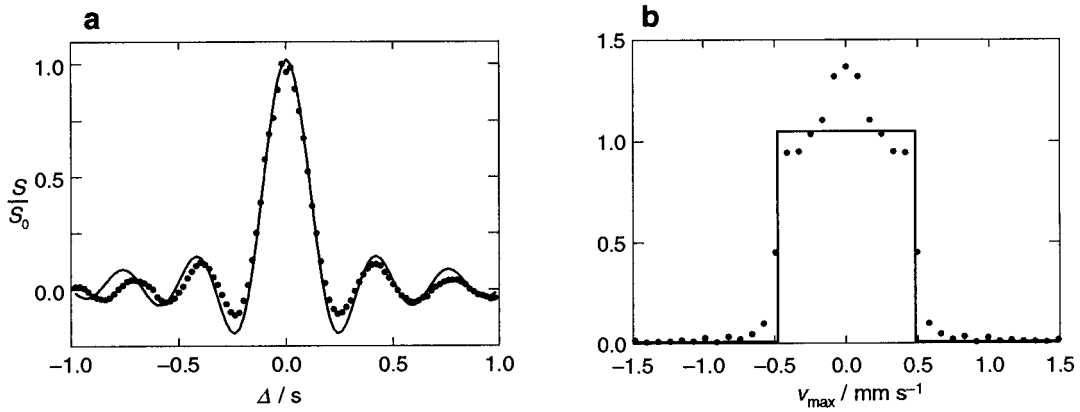


**FIG. 3.** Plot (a) shows, as dots, the measured signal attenuation, as a function of the time $\Delta$ ($\Delta = \tau_{m,1} - \tau_{m,2}$), recorded using the sequence of Fig. 1c; as described in the text, provided that the sum of the two mixing times is constant, the signal decay is attributable solely to convection. The sinc-like profile of the decay is clearly visible; the solid line is a best-fit sinc function. Plot (b) shows, as dots, the velocity distribution which can be deduced by Fourier transformation of the time decay shown in (a). The square distribution, shown by the solid line in (b), is determined from the best-fit sinc function shown in (a).

of convection velocities present, but that the real distribution is by no means flat.

Convection is essentially a thermally driven process and also depends on the detailed physical properties of the solvent. Generally, less viscous solvents are expected to show faster convection. Figure 4a shows data for convection velocities (expressed as $v_{max}$ values based on fitting the signal decay with a sinc function) as a function of temperature for three different solvents: DMSO, $H_2O$, and $CHCl_3$. In each case the signal monitored was from the protonated form of the deuterated solvent. As expected, the convection velocity rises quite steeply with temperature, approximately doubling for a 5–10 K rise in temperature. Chloroform, because it is significantly less viscous than DMSO or water, shows more than an order of magnitude faster convection.

The convection velocity is also affected by the gas flow rate through the variable temperature unit; Fig. 4b gives some representative results for the three solvents. It is seen that the velocity of convection does depend on the flow rate, appearing to increase quite markedly at rates below approximately 300 liters $h^{-1}$ (the data in Fig. 3a were taken at a flow rate of 450 liters $h^{-1}$). Presumably at the lower flow rates there is insufficient thermal capacity in the gas to maintain a constant temperature across the sample. These results point to the importance of ensuring adequate gas flow, and give a method of assessing whether or not the flow is adequate.

Decoupling, particularly broadband decoupling of a heteronucleus such as $^{13}C$, requires quite high power irradiation and this can cause direct heating of the sample. Figure 5 shows the effect of such irradiation on $^{13}C$ at two different power levels

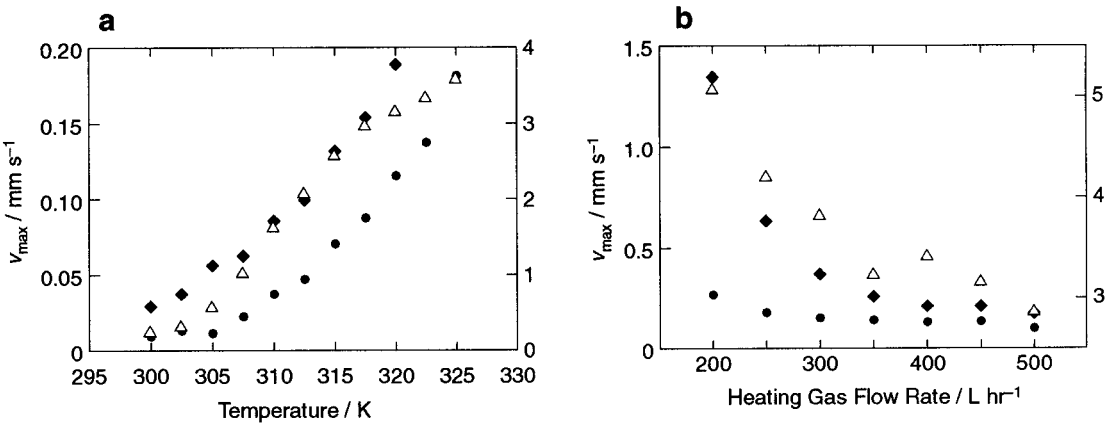


**FIG. 4.** Maximum convection velocities, determined using the sequence of Fig. 1c followed by fitting of the data to a sinc function, for different combinations of solvent and gas flow rate through the temperature regulator. The closed circles are for $H_2O$ and the closed diamonds are for DMSO; these points refer to the left-hand scale. The open triangles are for $CHCl_3$, and these refer to the right-hand scale. The data shown in plot (a) were recorded at a flow rate of 450 liters $h^{-1}$ and show the variation of convection velocity with temperature. The data shown in plot (b) were recorded at a temperature of 320 K and show how the convection velocity varies with gas flow rate. In each case the sample consisted of a small amount of the protonated form of the corresponding deuterated solvent.

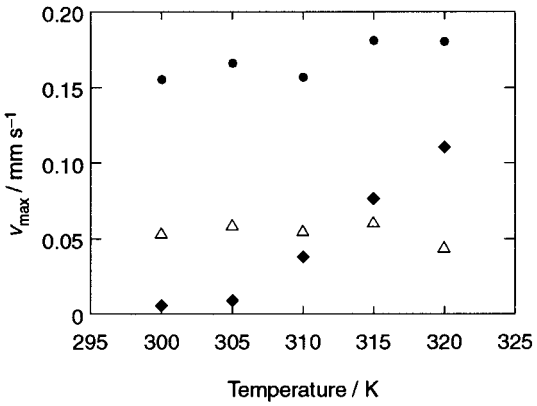


**FIG. 5.** Maximum convection velocities for $H_2O$ (in $D_2O$), determined and plotted as for Fig. 4; the gas flow rate was 450 liters $h^{-1}$. The closed diamonds were measured in the absence of $^{13}C$ decoupling, the open triangles were measured with a decoupler power of approximately 1.5 W (18 dB below the maximum power available), and the closed circles were measured with a power of approximately 6 W (12 dB below the maximum).

typical of those needed for broadband decoupling. The duty cycle of the decoupling was 30%. Irradiation at the higher power level causes a dramatic increase in the convection velocity, to the extent that the underlying variation with temperature is swamped. At the lower power level there is still a significant effect, although, somewhat curiously, at the higher temperatures the convection velocity is lower than that found when no decoupling is applied. These results show that the variable temperature unit is incapable of compensating for uneven heating caused by decoupling, and further underline the continued need for power-efficient decoupling methods.

*Temperature Profiles*

For the imaging pulse sequence of Fig. 1d typical parameters involved incrementing the gradient (length 150 $\mu$s) from $-23$ to $+23$ G $cm^{-1}$ in 256 steps. After Fourier transformation this gives a slice thickness of 170 $\mu$m. All measurements were made using HTmDOTP dissolved in $D_2O$. Data are plotted for the region $\pm 0.4$ cm from the center of the sample; slices corresponding to greater distances had insufficient signal in them to allow a reliable estimate of the temperature to be made.

Figure 6a shows the effect of varying the temperature at a low gas flow rate of 200 liters $h^{-1}$. The first point to note is that the average sample temperature deviates significantly from the temperature set on the variable temperature controller. This is perhaps not surprising, given that the thermocouple used by the variable temperature unit is outside the sample. At the highest temperature (325 K) there is a gradient of almost 1 K across the sample, with the top (positive $z$) cooler than the bottom. Such a situation is expected to lead to convection, and this correlates with the high convection rates found for such flow rates (see Fig. 4b). At lower temperatures the gradient is much smaller, becoming barely perceptible at 300 K. It is interesting to note that at 315 K the ends of the sample are cooler than the middle, and at lower temperatures the top of the sample is hotter than the bottom (this is particularly noticeable at 310 K). Such a temperature inversion is not expected to give rise to convection, at least on a scale comparable to that found for a profile in which the temperature decreases going up the tube. It should be noted that because only $z$-gradients are used, this experiment measures the *average* temperature in a slice, thus masking any variations that occur in the transverse direction. This

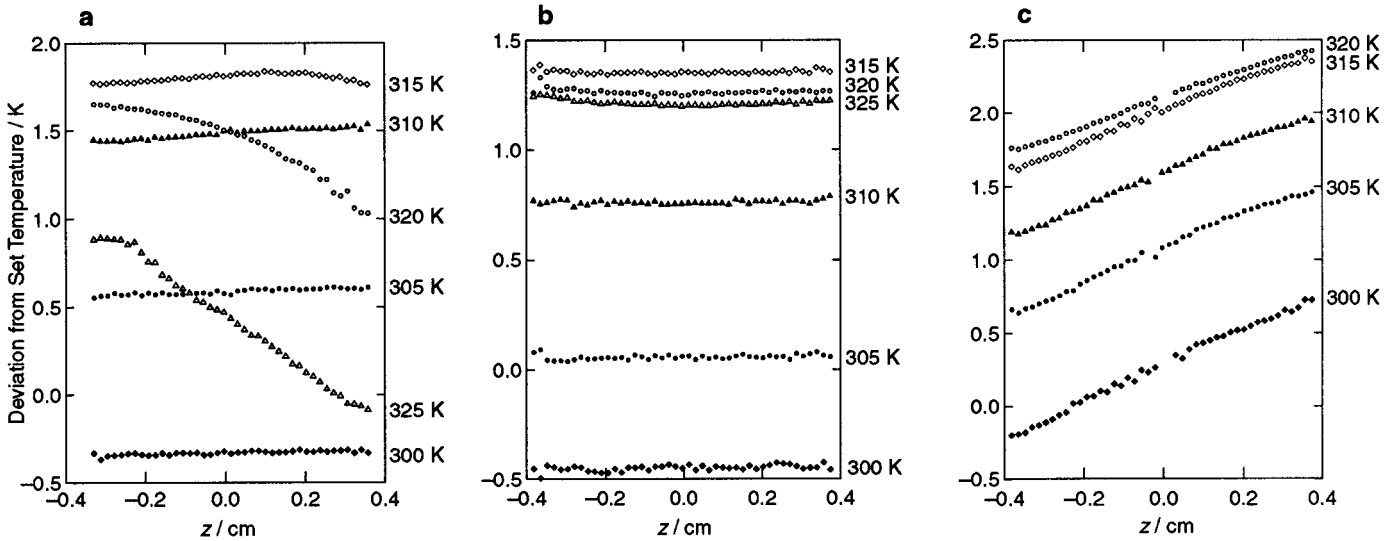


**FIG. 6.** Temperature profiles determined using the chemical shift imaging sequence of Fig. 1d in conjunction with HTmDOTP, whose spectrum is strongly temperature dependent. All the data were recorded in $D_2O$ and for various temperatures as indicated on the plots. The data in plot (a) were recorded with a flow rate of 200 liters $h^{-1}$, whereas those in plot (b) were recorded with a flow rate of 450 liters $h^{-1}$. The data in plot (c) were recorded at the higher flow rate, but with broadband $^{13}C$ decoupling at the 18 dB level (see caption to Fig. 5).

may explain why there is convection in cases where it *appears* that the temperature increases in the *z*-direction.

Increasing the flow rate to 450 liters $h^{-1}$ greatly reduces the temperature gradients, as is seen in Fig. 6b. These results are in line with the convection rate measurements, which also show that the higher gas flow rate minimizes convection.

Finally, Fig. 6c shows the effect of $^{13}C$ decoupling at the lower power level, as described in the previous section. Even though the gas flow rate is 450 liters $h^{-1}$, decoupling results in the generation of significant temperature gradients across the sample, in line with the increased convection noted above (see Fig. 5). Once more, the temperature appears to increase up the sample tube; the effect is most pronounced at the lower temperatures.

## CONCLUSIONS

We have developed a simple method for measuring the velocity profile within an NMR sample; our method is straightforward to use and has the particular advantage of separating cleanly the effects of convection from those of diffusion and relaxation. We have also shown how a simple chemical shift imaging sequence, combined with a suitable molecule with a highly temperature sensitive spectrum, can give detailed data on the temperature profile within the tube.

It should be noted that, in contrast to diffusion, whose rate depends on molecular size, convection is primarily a function of the solvent. Thus, for a given solvent, all solutes are equally affected, regardless of their size.

Using these methods, it has been shown that there are significant temperature gradients within an NMR sample, and that these lead to convective flow. The gradients can be minimized by increasing the gas flow through the variable temperature system. It is also shown that high-power decoupling leads to increased temperature gradients and convection, even at high gas flow rates through the VT system. These data, and the methods used for their measurement, should be of interest to those involved in assessing and developing new probes and temperature control units, as well as to those interested in determining whether or not convection is a significant source of signal loss in their experiments.

## ACKNOWLEDGMENTS

We thank David Neuhaus (MRC Laboratory of Molecular Biology, Cambridge) for a generous allocation of spectrometer time and his continuing interest in this project; Norbert Müller (Johannes Kepler University, Linz) for kindly supplying a preprint of Ref. (*3*); A. Dean Sherry (Southwestern Medical Center, University of Texas) for a generous gift of a sample of HTmDOTP; and Daniel Marek (Bruker, Fällenden) for helpful discussions. N.M.L. thanks the Churchill Foundation and the National Science Foundation for support. This material is partly based on work supported under a National Science Foundation Graduate Research Fellowship.

## REFERENCES

1. A. Allerhand, R. E. Addleman, and D. Osman, Ultra-high-resolution NMR. I. General considerations and preliminary results for $^{13}C$ NMR, *J. Am. Chem. Soc.* **107,** 5809–5810 (1985).
2. S. R. Maple and A. Allerhand, Ultra-high-resolution NMR. IV. A simple technique for measurements of sample temperature gradients, *J. Magn. Reson.* **66,** 168–171 (1986).
3. A. Jerschow and N. Müller, Suppression of convection artifacts in stimulated echo diffusion experiments: Double stimulated echo experiments, *J. Magn. Reson.* **125,** 372–375 (1997).
4. A. Jerschow and N. Müller, Convection compensation in gradient enhanced nuclear magnetic resonance spectroscopy, *J. Magn. Reson.* **132,** 13–18 (1998).
5. P. T. Callaghan, "Principles of Nuclear Magnetic Resonance Microscopy," Oxford Univ. Press, Oxford (1993).
6. T. R. Brown, B. M. Kincaid, and K. Ugurbil, NMR chemical shift imaging in three dimensions, *Proc. Natl. Acad. Sci. U.S.A.* **79,** 3523–3526 (1982).
7. C. S. Zuo, K. R. Metz, Y. Sun, and A. D. Sherry, NMR temperature measurements using a paramagnetic lanthanide complex, *J. Magn. Reson.* **133,** 53–60 (1998).